






Article

Wear Resistance of Plasma Electrolytic Oxidation Coatings on Ti-6Al-4V Eli Alloy Processed by Additive Manufacturing

Pedro Bell Santos ¹, Victor Velho de Castro ¹, Estela Kerstner Baldin ^{1,*}, Cesar Aguzzoli ²,
Guilherme Arthur Longhitano ^{3,4}, André Luiz Jardim ^{3,4}, Éder Sócrates Najar Lopes ^{3,5},
Antonio Marcos Helgueira de Andrade ⁶ and Célia de Fraga Malfatti ¹

- ¹ LAPEC—Universidade Federal do Rio Grande do Sul (UFRGS)—Avenida Bento Gonçalves, Porto Alegre 91501-970, RS, Brazil; pedro.bell@acad.pucrs.br (P.B.S.); victorvcastro@yahoo.com.br (V.V.d.C.); materiaisxenergia@gmail.com (C.d.F.M.)
- ² PGMAT—Programa de Pós-graduação em Engenharia de Materiais (PGMAT), Universidade de Caxias do Sul—Rua Francisco Getúlio Vargas, Caxias do Sul 95070-560, RS, Brazil; caguzzol@ucs.br
- ³ BIOFABRIS—Instituto de Biofabricação (INCT-BIOFABRIS)—Av. Albert Einstein, Campinas 95070-560, SP, Brazil; guilonghita@gmail.com (G.A.L.); ajardini@unicamp.br (A.L.J.); ederlopes@fem.unicamp.br (É.S.N.L.)
- ⁴ FEQ—Faculdade de Engenharia Química, Universidade Estadual de Campinas (UNICAMP)—Avenida Albert Einstein, Campinas 13083-852, SP, Brazil
- ⁵ FEM—Faculdade de Engenharia Mecânica, Universidade Estadual de Campinas (UNICAMP)—Rua Mendeleyev, Campinas 13083-860, SP, Brazil
- ⁶ Instituto de Física, Universidade Federal do Rio Grande do Sul (UFRGS)—Avenida Bento Gonçalves, Porto Alegre 91501-970, RS, Brazil; antonio.andrade@ufrgs.br
- * Correspondence: estelakerstner@gmail.com



Citation: Santos, P.B.; de Castro, V.V.; Baldin, E.K.; Aguzzoli, C.; Longhitano, G.A.; Jardim, A.L.; Lopes, É.S.N.; de Andrade, A.M.H.; de Fraga Malfatti, C. Wear Resistance of Plasma Electrolytic Oxidation Coatings on Ti-6Al-4V Eli Alloy Processed by Additive Manufacturing. *Metals* **2022**, *12*, 1070. <https://doi.org/10.3390/met12071070>

Academic Editor: Massimo Pellizzari

Received: 3 May 2022

Accepted: 20 June 2022

Published: 23 June 2022

Publisher's Note: MDPI stays neutral with regard to jurisdictional claims in published maps and institutional affiliations.



Copyright: © 2022 by the authors. Licensee MDPI, Basel, Switzerland. This article is an open access article distributed under the terms and conditions of the Creative Commons Attribution (CC BY) license (<https://creativecommons.org/licenses/by/4.0/>).

Abstract: The additive manufacturing (AM) technique can produce Ti-6Al-4V ELI (extra low interstitial) alloy for personalized biomedical devices. However, the Ti-6Al-4V ELI alloy presents poor tribological behavior. Regarding this, coatings are a feasible approach to improve the wear resistance of this alloy. In the literature, the tribological behavior of TiO₂ coatings incorporated with Ca and P formed by one-step plasma electrolytic oxidation (PEO) on Ti-6Al-4V ELI alloy processed by AM has not been investigated. Thus, in the present work, it was studied the influence of Ti-6Al-4V ELI alloy processed by AM on the wear resistance and morphologic of the coating obtained by PEO (plasma electrolytic oxidation). In this way, three different voltages (200, 250, and 300 V) were employed for the PEO process and the voltage effect on the properties of the coatings. The coatings were characterized by contact profilometry, scanning electron microscopy, energy-dispersive spectroscopy, the sessile drop method, grazing-incidence X-ray diffraction, and wear tests, on a ball-on-plate tribometer. The increase in applied voltage promoted an increase in roughness, pore area, and a decrease in the pore population of the coatings. In addition, the coatings, mainly composed of anatase and rutile, showed good adhesion to the metallic substrate, and the presence of bioactive elements Ca and P were detected. The thickness of the coatings obtained by PEO increases drastically for voltages higher than 250 V (from 4.50 ± 0.33 to 23.83 ± 1.5 μm). However, coatings obtained with lower voltages presented thin and dense layers, which promoted a superior wear resistance (increase in wear rate from 1.99×10^{-6} to 2.60×10^{-5} mm^3/s). Finally, compared to the uncoated substrate, the PEO coatings increased the wear resistance of the titanium alloy obtained by AM, also showing a superior wear resistance compared to the commercial Ti-6Al-4V alloy previously evaluated, being such a positive and promising behavior for application in the area of metallic implants.

Keywords: powder bed fusion; DMLS; surface functionalization; osseointegration; bioactive surface

1. Introduction

Additive manufacturing (AM), also known as rapid prototyping or 3D printing, has been largely applied in different industries, including construction, prototyping, jewelry,

aerospace, automobilism, medicine, biomechanical, and biomedical, among others [1]. The direct metal laser sintering (DMLS) technique is one of the many techniques of AM for metallic materials. It belongs to the powder bed fusion (PBF) category, which has been defined by ISO/ASTM 52900 [2] as an “additive manufacturing process in which thermal energy selectively fuses regions of a powder bed”. Therefore, this technology is appropriate for fine metallic powders selective fusion by laser and to produce dense metallic parts, due to its good surface and geometric finish and reuse of powder [3,4]. Recent publications have presented the advantages of the additive manufacturing process compared to conventional manufacturing, as well as the importance of evaluating different operating conditions to obtain, in addition to customization, better precision, and better mechanical properties of the components manufactured by this process [5–7]. Furthermore, Khorasani et al. (2021) showed significant reductions in AM processing costs compared to the conventional machining technique [8]. Titanium and its alloys are extremely used in biomedical applications such as orthopedic, cranial, and dental implants; Ti has a high load-bearing capacity, biocompatible response, elevated specific weight ratio, and chemical stability [9,10]. The laser powder bed fusion (L-PBF) process can be utilized as a tool for directly producing personalized biomedical devices in titanium alloys (Ti-6Al-4V), allowing a reduction in the surgical process time, as well as the infection and rejection risks, anesthesia time, and the risk for the patient—all this with low costs [11].

Ti-6Al-4V has been exhaustively used as an implantable material. However, their fretting and abrasive behavior, coefficient of friction, and wear resistance are poor when compared to other conventional alloys used for orthopedic biomaterials as cobalt-based alloys and stainless steel, in hip replacement and other artificial joints [12,13]. Therefore, the wear behavior of Ti-6Al-4V plays a key role when this material is implanted as a biomaterial responsible for fixating a fracture or working as an artificial joint, due to the relative movements between two different materials such as the implant and the bone. Improving the tribological behavior of Ti-6Al-4V will enable better biocompatibility and longer useful life of the implant [14].

Titanium implants are treated superficially, for use in the area of tissue regeneration, to improve their tribological, anticorrosive, biological, and mechanical properties [15–18]. The plasma electrolytic oxidation (PEO) process, also called micro-arc oxidation (MAO), emerges as an applicant capable of complementing and attributing such properties to Ti-6Al-4V implants [19,20]. The PEO process consists of the principle of anodic oxidation of valve metals in aqueous alkaline, and corrosive electrolytes in the plasma discharge region at exceeding the critical values of the polarization potential on metals [21]. PEO coatings have a characteristic, rough porous morphology and great thickness, due to the micro-discharges evolved in the coatings mechanism formation, enabling the cells’ adhesion and posterior proliferation [22]. Anatase and rutile are the main phases formed in coatings obtained with PEO, on Ti-6Al-4V. In terms of proliferation and adhesion of osteoblasts, the anatase has been related as a phase with better cytocompatible behavior [23], while the rutile phase shows a greater hardness than those cited before, in addition to having wear and low friction reduction properties [24]. The combination of both in the PEO coatings demonstrated an excellent response regarding the electrochemical and tribological properties by decreasing the corrosion and the mechanical damage [25]. Furthermore, PEO coatings have superior hardness in comparison to the substrate and, therefore, superior tribological behavior [26].

The PEO process enables the incorporation of P- and Ca- bioactive elements into the chemical composition of the coatings; this incorporation has been related as capable of enhancing the biological response of the Ti-6Al-4V and inducing osseointegration, as Santos et al. [27] show in their work. Yu and Choe [28] demonstrate that PEO coatings composed of Ca/P and TiO₂, formed on Ti-6Al-4V substrate, were capable to induce the formation of hydroxyapatite (HA) by immersion in SBF, which exhibits superior bioactivity when compared with the naked substrate [21]. The biological response of PEO coatings, combined with a hydrothermal layer of HA, obtained on Ti-6Al-4V substrate produced

by additive manufacture techniques, was evaluated by Fazel et al. [29]. According to the authors, the coatings showed a biological response facilitating the proliferation and osteogenic differentiation of cells.

Yan et al. [30] analyzed the wear resistance of PEO coatings on samples of Ti-6Al-4V, manufactured by selective laser melting (SLM) technology, using an aluminate-based electrolyte. Aluminum, the main element present in aluminates, has known toxic activity in the human body [31,32], making the application of this type of electrolyte unfeasible for orthopedic implants, for example. Their results indicated a tendency to reduce the wear rate by increasing the time to obtain the coating by applying a duty cycle of 0.5 [30]. Hussein et al. [33,34] propose the occurrence of the fourth stage of PEO coatings formation, which arises in longer treatment times. Sparks developed during this stage are more concentrated, larger, and have a longer lifespan. This can lead to irreversible damage to the coating. According to Han [35], the application of high duty cycles can reduce the growth rate of the PEO coatings, due to the destructive effect caused. Using high duty cycles leads to elongation of the pulses, inducing a massive release of energy, resulting in the development of structures with larger pores due to coarse-grained graining with the possible formation of cracks. Therefore, the variation of other parameters for obtaining the coating in the search for the optimization of properties is more suitable [27].

Wu et al. [36] investigate the properties of PEO coatings formed on SLM Ti-6Al-4V alloy and the microstructure influence on growth behavior, showing that the coatings formed on the substrate produced by the SLM technique have fewer defects, small size pores, and major thickness than that forming in commercial Ti-6Al-4V alloy. However, the authors have carried out no tribological test. The tribological behavior of TiO₂ coatings with the incorporation of –P and –Ca ions formed by the one-step PEO method on Ti-6Al-4V ELI alloy processed by L-PBF has not been investigated in the literature.

The main goal of this study is to investigate the wear behavior in PEO coatings obtained onto Ti-6Al-4V ELI samples, produced by the L-PBF technique, applying the same PEO process parameter from the previous authors' paper [27], adding a new electrical parameter and a new duty cycle of 0.385, aiming in a better wear response. Moreover, the surface and morphological characteristics of the coatings have also been evaluated.

2. Materials and Methods

2.1. Obtaining Samples

Ti-6Al-4V ELI cylindrical samples with 5 mm height and 25 mm diameter were produced by L-PBF as previously reported [37].

2.2. Obtaining Coatings

The PEO coatings in the samples were obtained as reported in previous works [27,38]. At the end of the voltage ramp, the electrical voltage is applied for 10 min with a duty cycle of 38.5% and a frequency of 300 Hz. The maximum values of positive and negative voltages are demonstrated below: 200/–16 V (TiAM-PEO_{200v}), 250/–20 V (TiAM-PEO_{250v}), and 300/–24 V (TiAM-PEO_{300v}). The voltage was increased at the rate of 1/–0.08 V/s, been the process started at 100/–10 V voltage.

2.3. Characterization

The samples for microstructural characterization were mechanically ground, polished, and etched with Kroll reagent 5% vol HNO₃ (Sigma-Aldrich, Sao Paulo, Brazil), 10% vol HF (Merck, Sao Paulo, Brazil) in H₂O, made at the Corrosion Research Laboratory (LAPEC) at the Federal University of Rio Grande do Sul (Porto Alegre, Brazil). Micrographs were recorded on a Leica DM IL LED light optical microscope (LOM; Wetzlar, Germany).

A TESCAN-Mira3 high-resolution scanning electron microscope (SEM/FEG) (Tescan, Czech Republic) was utilized to analyze the morphology of the formed coatings. The grazing-incidence X-ray diffraction analysis (GIXRD) was performed in a Bruker D8 ADVANCED diffractometer (Bruker, Germany) (Cu-K α incident radiation, $\lambda = 0.15418$ nm),

and measurements were conducted with an incidence angle of 1.5° and the GID patterns were recorded with a step size of 0.02° over the range $15\text{--}75^\circ$. Using the Image J software (version 1.53a, National Institute of Health, Bethesda, MD, USA) package and images obtained by SEM, the quantification of the surface porosity of the coatings was performed. The micrometric roughness (R_a and R_z) measurements were made in a profilometer (Model 112, Taylor Hobson, Leicester, UK).

The PEO coating wettability was made by contact angle measurements using the sessile drop method on a device designed by the Corrosion Research Laboratory (LAPEC) at the Federal University of Rio Grande do Sul (Porto Alegre, Brazil). The contact angle was measured with water in a goniometer, using a low magnification lens.

A ball-on-plate tribometer, model UMT-3, (CETR, Campbell, CA, USA), controlled through software was used to perform the wear test. Ytria stabilized zirconia spheres with 5 mm diameter were used as a counter-body. A load of 1 N for 4 h was used at a frequency of 3 Hz with a stroke length of 3.0 mm. The worn tracks were characterized by contact profilometry XP-2 Profiler (Ambios, Santa Cruz, CA, USA) and SEM/FEG.

3. Results and Discussion

Figure 1 shows the SEM/FEG images of the surface morphology after the PEO treatment condition. The TiAM-PEO_{250v} and TiAM-PEO_{300v} samples showed a porous volcanic vent morphology, while the TiAM-PEO_{200v} samples demonstrate a well-defined porous morphology. All the coatings produced have a brown coloration because of the high phosphate concentration in the electrolyte [39]. Nevertheless, the presence of cracks was noted in all the PEO coatings. The increase in the crack quantity grew with the increase in the final applied voltage and time process, in accordance with work by Durdu et al. [40] with PEO coatings on commercial Ti-6Al-4V alloy [27].

The increase in the final voltage led to the increase in the roughness (R_a , R_z), thickness, pore area, and decrease in pore population, as shown in Figure 1 and Table 1, that exhibit cross-sectional morphology and the surface properties of the samples, respectively. This response was already seen in a previous work of the authors on the commercial Ti-6Al-4V alloy substrate [27].

Table 1. Surface characteristics (roughness, thickness, and porosity).

Sample/Properties	Ti6Al4V-AM	TiAM-PEO _{200v}	TiAM-PEO _{250v}	TiAM-PEO _{300v}
R_a (μm)	0.13 ± 0.02	0.17 ± 0.04	0.28 ± 0.01	0.72 ± 0.05
R_z (μm)	1.3 ± 0.62	1.50 ± 0.36	2.33 ± 0.32	4.55 ± 0.28
Layer thickness (μm)	-	2.05 ± 0.13	4.50 ± 0.33	23.83 ± 1.5
Outer layer (μm)	-	1.53 ± 0.26	3.64 ± 0.44	22.53 ± 1.25
Inner layer (μm)	-	0.41 ± 0.04	0.69 ± 0.18	1.16 ± 0.22
Pore population density (pores. mm^{-2})	-	17.9×10^4	10.0×10^4	50.4×10^3
Greater pore area (μm^2)	-	1.62	5.32	18.31
Smaller area pore (μm^2)	-	0.06	0.07	0.11

The coatings obtained on the substrate produced by L-PBF show greater thickness than the coatings obtained on the commercial Ti-6Al-4V alloy [27], in addition to demonstrating a larger population of pores and smaller area. This different response could be related to the microstructure of the substrate produced by the L-PBF technique (Figure 2), since fine-grained substrates produced by mechanical treatments, such as channel angular pressing (ECAP), reduce the pore diameter whereas enhancing the thickness compared to coarse-grained samples and increasing growth rate improve the reactivity of the surface, reduce discharge size and enhance the discharge density, on the PEO process [41,42]. As noted by Longhitano et al. [37], the substrate obtained by the L-PBF process presents an acicular martensitic structure constituted by α/α' . Considering that, while the fabrication process takes place, a rapid cooling rate is resulted from the quick interaction between the laser and the surface of the molten material, promoting a refined martensitic structure inside prior

β grains due to the abrupt cooling from the β phase field. In contrast, the commercially annealed Ti-6Al-4V alloy has $\alpha + \beta$ phases equiaxial microstructure, with grain size larger than that obtained by the L-PBF process. According to Wu et al. [36], the non-equilibrium phases in the additively manufactured Ti-6Al-4V substrate have a larger number of grain boundaries, due to its small grain size, providing more nucleation sites for the passive film in the initial stage of the PEO process. Moreover, the high-energy grain boundaries and other microstructural defects, arising from the microstructure obtained at high cooling rates, promoted a higher growth rate of the coatings obtained over the AM process, due to the storage of excess energy to accelerate the kinetics of the chemical reaction with smaller amounts of microcracks.

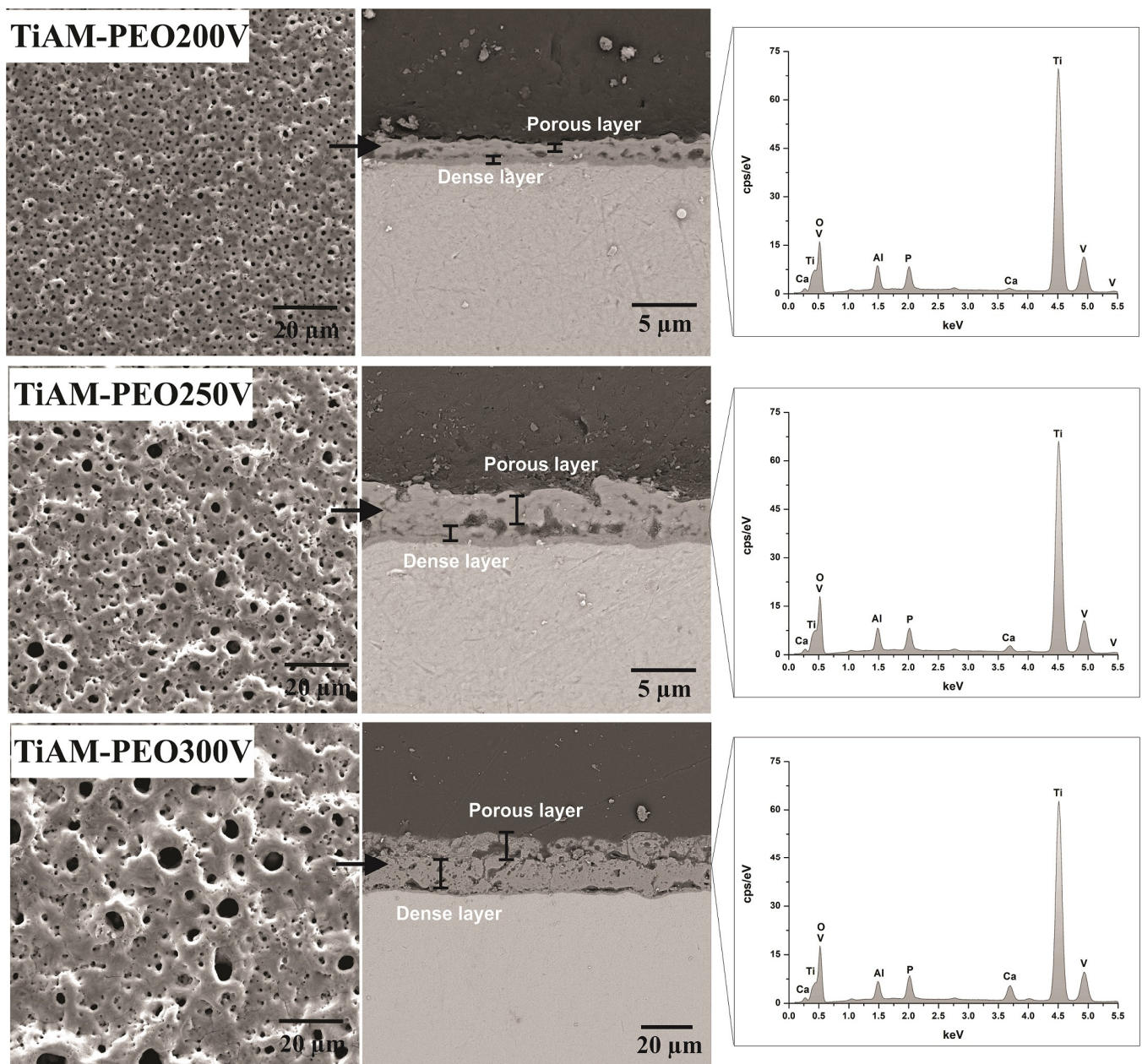


Figure 1. SEM/FEG images of top morphology, cross-sectional morphologies of the PEO coatings PEO on Ti-6Al-4V ELI alloy processed by L-PBF and surface EDS spectrogram.

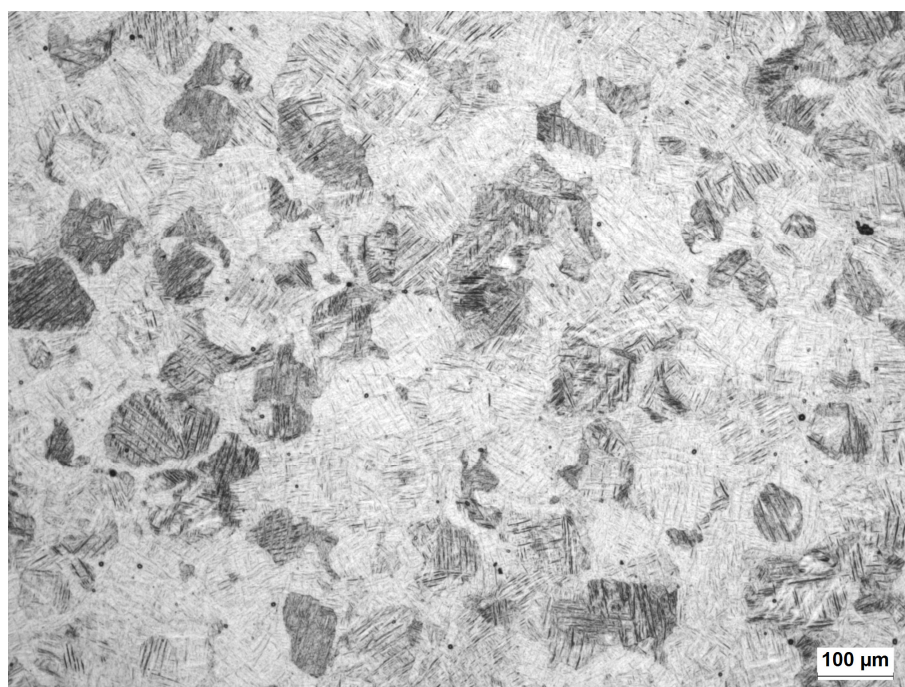


Figure 2. LOM micrograph of Ti-6Al-4V ELI alloy processed by L-PBF. The microstructure is composed of an acicular martensitic structure in prior β grains.

The three samples had formed coatings that were extremely well attached to the AM substrate composed of two different layers, one dense inner layer, and a porous outer layer, as seen in Figure 1. This result agrees with those found by Fazel et al. [29] in their work on PEO coatings obtained on Ti-6Al-4V alloy processed by the L-PBF technique. The inner layer, which grows direct into the metal under high pressures and temperatures, is dense, crystalline, and firmly attached to the substrate. However, the outer layer is amorphous due to the high cooling rate promoted by the electrolyte, with a complex and porous morphology formed by the existence of micro discharges caused during the formation of PEO coatings [42,43]. Moreover, the TiAM-PEO_{200v} and TiAM-PEO_{250v} samples presented denser coatings, showing a hollowed structure, in relation to the coating formed at sample TiAM-PEO_{300v}, which showed a thicker coating, with a sponge-like mixed with a hollowed structure [44]. There was no major difference in the thickness of the inner layer of the samples. Although, there was in the thicknesses of the outer layer because of the increase in the final applied voltage, as seen in Table 1.

The presence of the elements Ti, Al, V, O, P, and Ca are observed in the PEO coatings' chemical composition by EDS analysis (Figure 1). The sparking phenomenon allows intense incorporation of Ca and P ions into the coatings, as these species primarily remain as amorphous phases or dissolved ions inside the PEO coatings [45]. P is well distributed through the thickness of the coating, while Ca is usually located on the surface of the coating and slowly lose concentration towards the inner region of the coating [46]. Those incorporated ions improve the surface bioactivity since Ca²⁺ cations migrate to the outer surface, which induces the formation of apatite in presence of OH⁻ and PO₄³⁻ (in biological media [47]). Furthermore, according to dos Santos et al. [48], the release of Ca²⁺ and PO₄³⁻ encourages the attraction of protein to these active sites and hydrolysis, exciting differentiation and proliferation of cells.

Figure 3A illustrates the grazing incidence X-ray diffraction patterns of the uncoated Ti-6Al-4V ELI alloy and the PEO coatings produced at different electrical parameters.

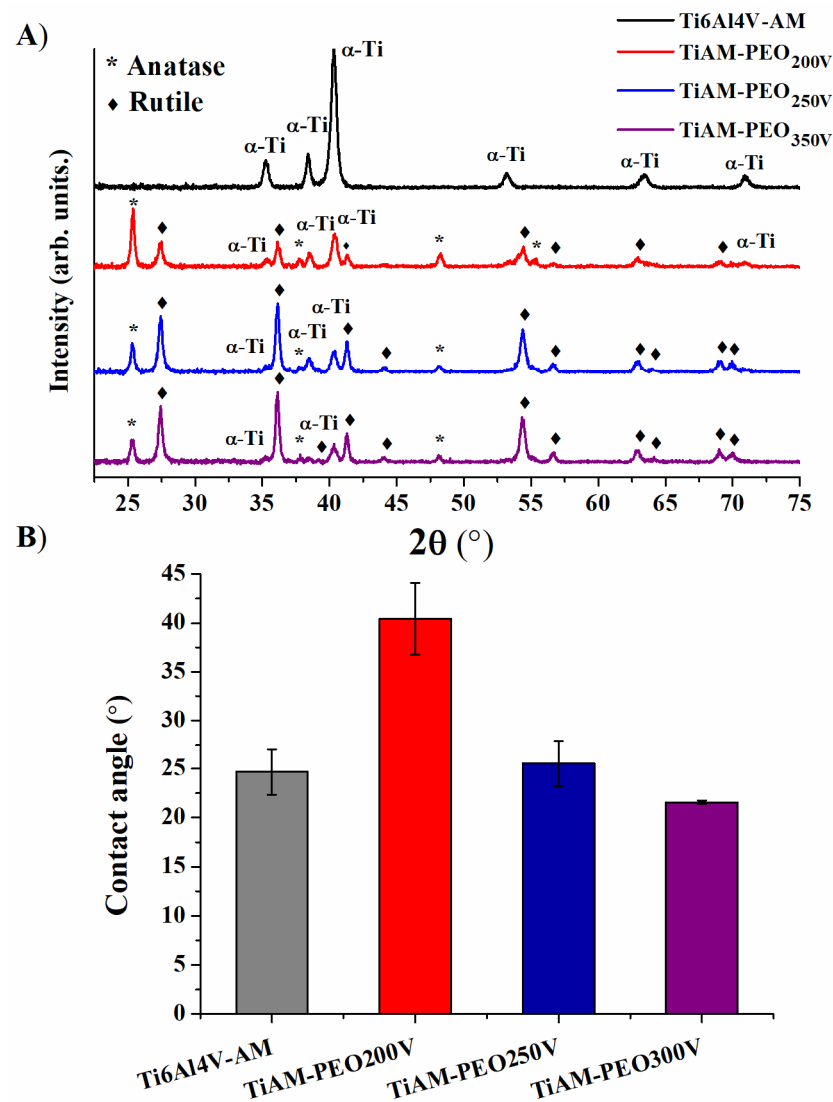


Figure 3. (A) Grazing incidence X-ray patterns of PEO coatings and (B) Contact angle values obtained for PEO coatings on Ti-6Al-4V ELI alloy processed by L-PBF.

The GIXRD analysis indicates the formation of coatings composed of two different phases of TiO_2 oxide: anatase (JCPDS NO. 01-084-1286)— TiO_2 and rutile (JCPDS NO.01-077-0442)— TiO_2 phases; only Ti α -phase peaks were detected on Ti-6Al-4V ELI alloy processed by L-PBF. The increase in the applied voltage in the samples increases the intensity of the peaks relative to the rutile phase and a decrease in peaks related to the anatase phase, as seen in previous authors' work [27]. This occurs due to the formation energy of both TiO_2 phases since the anatase phase requires lower energy to be formed, in relation to the rutile phase [49]. Rutile, between all the titanium phases, is well-known as the more resistant to wear because of its wear reduction and low friction properties [24,50]. However, anatase microcrystals have been used as an additive in lubricating oil improving the anti-wear performance [51]. Furthermore, Chen et al. [52] and Chung et al. [53] made comparisons between the anatase and rutile phases in PEO coatings obtained on Ti-6Al-4V alloy, their findings support the hypothesis that rutile overcomes anatase in terms of biocompatibility.

Through the sessile drop tests (Figure 3B) it was possible to verify a similar behavior of the PEO coatings in comparison to the AM metallic substrate, less in the TiAM-PEO_{200V} that showed the biggest contact angle. The contact angles measured in water for the coated samples decreased with the increase in the applied voltage. This behavior can be related to the bigger amount of rutile observed in XRD for TiAM-PEO_{300V}. According

to Mashtalyar et al. [54], it presents a more hydrophobic behavior, in accordance with the previously cited properties. This behavior could be explained by the increase in the roughness, with the presence of a large number of pores of greater size, and TiO_2 crystals quantity in the coatings, those crystals encourage the development of hydroxyl radical groups ($-\text{OH}$) on the surface, increasing the hydrogen bonding formations with water molecules [55–57]. Several studies have demonstrated that hydrophilic surfaces are more efficient for cells to attach than hydrophobic surfaces [58,59]. The close interaction that occurs due to the hydrophilic surfaces with biological fluids, enables the interaction of the cells receptors with the proteins, initially adsorbed on the surface [60].

The progress of the coefficient of friction (COF) during sliding of the AM substrate and different coatings produced by PEO against zirconia spheres is shown in Figure 4.

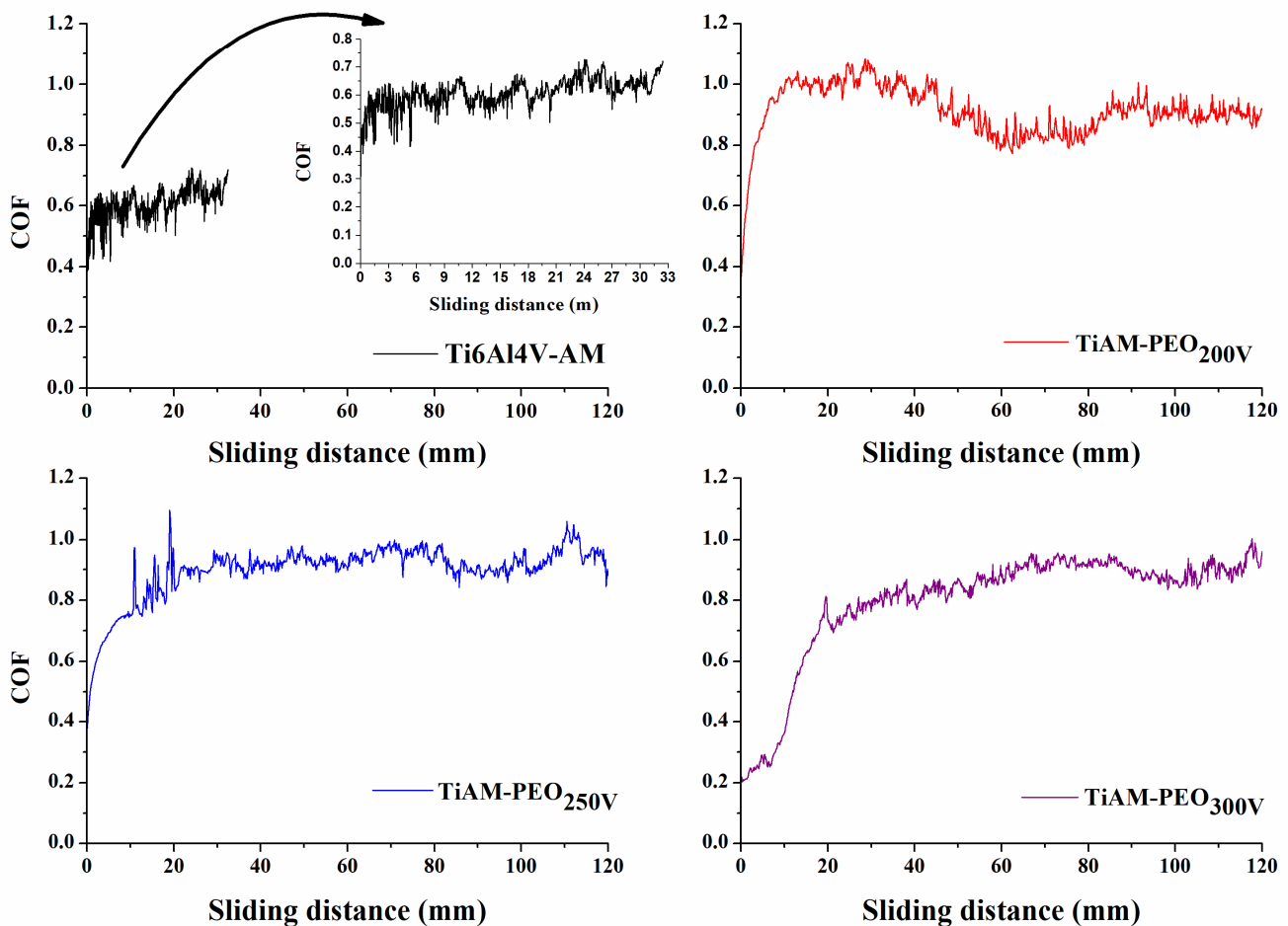


Figure 4. Coefficient of friction (COF) of coatings obtained by PEO on Ti-6Al-4V ELI alloy processed by L-PBF as a function of time (load of 1 N, frequency of 3 Hz, and stroke length of 3.0 mm, against body = zirconia sphere stabilized with yttria).

For the Ti6Al4V-AM sample (substrate) the COF values were in the range of 0.5–0.7 during the test of a duration of 32.4 m, of sliding, which is consistent with the literature data [30,61]. For all coated samples higher COF values were measured ranging from 0.7 to 1, being similar to that of Alves et al., in his study about PEO coatings obtained at commercial Ti-6Al-4V, using a solution rich in Ca^{2+} and P^{3-} [24]. The evolution of the rough surface of the coating to the smoother surface of the worn coating resulted in the initial variation of the COF [24,62]. The tests were stopped before 129.6 m of sliding for the coated samples. It was found that the COF values of the coated samples were influenced by the roughness values, morphology, and great hardness, in comparison with the substrate, due to the variance verified at the first meters of the test [24,62]. The values of hardness for the PEO

coatings vary between 400 and 600 HV [50], while the Ti6Al4V-AM sample shows values close to 332 HV, as found in an author's previous work [63]. The porous topography of the PEO coatings is firstly leveled, and the frictional forces become larger, conducting to the high COF [64]. In addition, the continuous fluctuation in the COF curves can be attributed to the roughness and the porous structure of the coatings, in addition, the adhesive wear contributes to the occurrence of this phenomenon [30]. Furthermore, the COF curves of the coated samples remained at levels higher than the COF of the substrate. This indicates that a complete disruption of the PEO coatings during the wear test did not occur.

The SEM/EDS analysis (Figure 5) shows the morphologies of the wear scars of the coated surfaces and the TiAM-Ti6Al4V sample and confirms the occurrence of abrasive wear in all the samples. Through the analysis of these images, the non-disruption of the layers of the coated samples was confirmed since no sliding wear marks lined with the pin track direction were noted, these marks are commonly correlated with the metallic material wear, or, in this case, substrate wear. For the TiAM-PEO_{200v} and TiAM-PEO_{250v} samples, it was noted that the coating outer layers present a relatively smooth worn morphology. The inner layers were not reached during the sliding test. Both TiO₂ phases, anatase and rutile, have lubricant and low friction properties, which can explain this type of wear behavior [43] after the smoothing of the wear scar.

This can be confirmed since the presence of pores behind the worn trail was verified, indicating that the zirconia ball was not able to fully wear the outer layer. Nonetheless, the TiAM-PEO_{300v} sample showed the formation of microcracks. According to Lawn et al. [65], material removal in hard and brittle solids is the mechanics of damage under micro and nano contacts and is directly related to the geometry of the body in contact with the brittle material. Normally, hard spheres generate predominantly elastic contacts with the formation of conical Hertzian cracks above a critical load. Those cracks gradually expand with the repeated sliding of the zirconia spheres on the surface of the coating, leading to delamination and localized coating disruption, as observed in Figure 5 [64]. It is important to note that microcracks occurred in the TiAM-PEO_{200v} and TiAM-PEO_{250v} samples, but in a lower magnitude that the cracks found on the TiAM-PEO_{300v} sample, with no delamination occurring. Durdu and Usta [43] indicate the possibility of these particles, produced through the wear test, acting as a lubricant between the coating and the wear ball. This phenomenon could take place in the TiAM-PEO_{200v} and TiAM-PEO_{250v} samples. However, as demonstrated by other authors [66] and by the work previously carried out by our research group [27], the tendency to increase COF can be caused by the third body formation because of material pullout generated by the localized delamination of the coating. Thus, this third body contributed to the increase in COF detected between 20 m and 80 m of distance covered in the test involving TiMA-PEO_{300v}. Furthermore, it may have contributed to the fluctuations in COF detected in the tests of the other samples.

The results of the SEM/EDS analysis of the wear balls used in the wear test are presented in Figure 6. A small amount of adhered material has been verified in all spheres used, leading to the conclusion that there was adhesive wear in all coated samples, in addition to the abrasive wear verified previously.

The results of the wear rate of the samples (Table 2) indicate, in addition to the superior behavior of the coatings in relation to the Ti6Al4V-AM sample, the more aggressive wear in the TiAM-PEO_{300v} sample ($2.60 \times 10^{-5} \text{ mm}^3/\text{s}$) in relation to the other two samples, TiAM-PEO_{200v} ($1.99 \times 10^{-6} \text{ mm}^3/\text{s}$) and TiAM-PEO_{250v} ($2.19 \times 10^{-6} \text{ mm}^3/\text{s}$). These results indicate that the density of the coatings, pore size (Table 1), and morphology (Figure 1) play a key role in the wear resistance. The two denser coatings (TiAM-PEO_{200v} and TiAM-PEO_{250v}) had lower wear rates concerning the TiAM-PEO_{300v}, which in turn shows a hollow-sponge mixed structure with larger pores due to the higher applied voltage that induces the formation of more intense discharges during the formation of PEO coatings. Regarding this, the TiAM-PEO_{200v} and TiAM-PEO_{250v} have a uniform energy distribution in the first phases of the formation of the coating, resulting in lower energy discharges and allowing fewer defects.

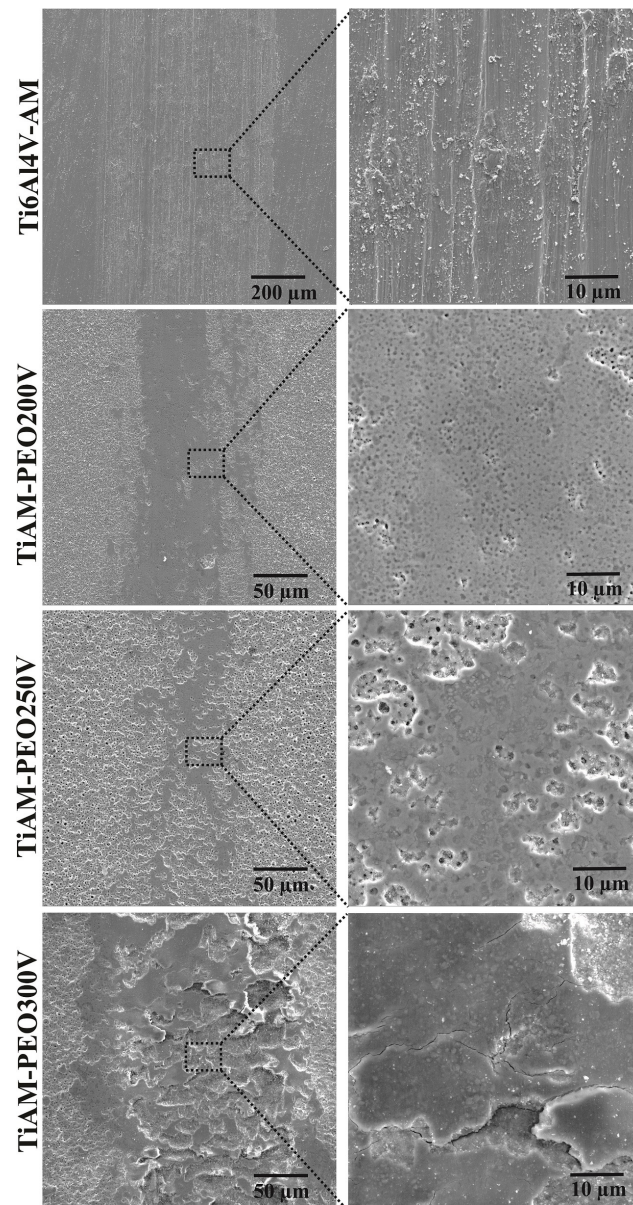


Figure 5. SEM/EDS of the wear tracks generated in the tribological test on coatings obtained by PEO on Ti-6Al-4-V ELI alloy additively manufactured.

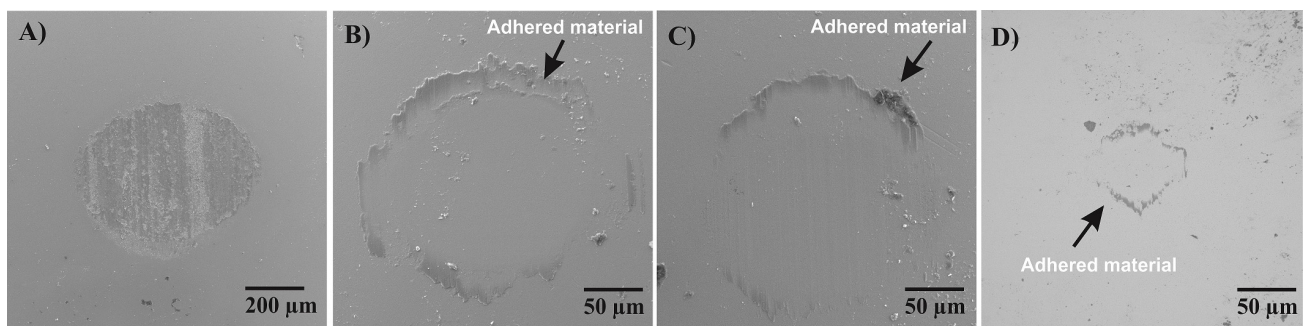


Figure 6. SEM/EDS of the Ytria stabilized zirconia spheres used during the tribological tests of the PEO coatings on Ti-6Al-4-V ELI alloy processed by L-PBF obtained in the different voltages: (A) Ti6Al4V-AM, (B) TiAM-PEO_{200V}, (C) TiAM-PEO_{250V} and (D) TiAM-PEO_{300V}.

Table 2. Breakage time and wear rate assessed after the abrasive wear test in ball-on-plate configuration for PEO coatings.

Sample	Sliding Distance (m)	Wear Rate (mm ³ /s)
Ti6Al4V-AM	32.4	9.79×10^{-5}
TiAM-PEO _{200v}	129.6	1.99×10^{-6}
TiAM-PEO _{250v}	129.6	2.19×10^{-6}
TiAM-PEO _{300v}	129.6	2.60×10^{-5}

In comparison with the PEO coatings studied previously by the authors [27] in Ti-6Al-4V commercial alloy, the COF values presented for the coatings formed on the L-PBF substrate have higher values. Nonetheless, the coatings formed on the substrate did not break during the sliding test like all the coatings produced on Ti-6Al-4V commercial alloy. This improvement in the wear resistance could be correlated to the major thickness and minor presence of defects of the PEO coatings obtained on the produced substrate. As hypothesized by Wu et al. [36], the small pore size of the PEO coatings obtained on the AM-produced substrate indicated the formation of fine discharges that contribute to an increase in oxidation time, thickening, and reduction in the formations of micro-cracks in the morphology of the coatings. Added to that, the reduction in the duty cycle (38.5%) compared to the previous article (51%) may have increased the life of the coatings during the wear test, since high duty cycle values lead to embrittlement, due to strong discharges with long life cycles that damage the coatings forming micro-cracks, leading to an increased mass loss of coatings during the wear test [67,68].

Even with the highest layer thickness ($23.83 \pm 1.5 \mu\text{m}$) among the studied samples, the TiAM-PEO_{300v} sample had the worst wear resistance due to its fragile outer layer that, when suffering abrasive wear, developed cracks that led to delamination. Not even the possible presence of larger amounts of rutile was able to give it better tribological properties compared to the other two coated samples [63]. Regarding the TiAM-PEO_{200v} and TiAM-PEO_{250v} samples, it can be stated that both had wear resistance very similar and superior to that demonstrated by the TiAM-PEO_{300v} samples, even though they were thinner, $2.05 \pm 0.13 \mu\text{m}$ and $4.5 \pm 0.33 \mu\text{m}$, respectively. Regarding the TiAM-PEO_{200v} and TiAM-PEO_{250v} samples, it can be stated that both had very similar and superior wear resistance to that demonstrated by the TiAM-PEO_{300v} samples, even though they were thinner, $2.05 \pm 0.13 \mu\text{m}$ and $4.5 \pm 0.33 \mu\text{m}$, respectively. This result is most likely related to the formation of a more compact layer, with smaller pores, in greater quantity and the rutile/anatase ratio.

4. Conclusions

The coatings obtained by the PEO process on the Ti-6Al-4V ELI substrate processed by L-PBF demonstrated a typical porous structure. The increase in applied voltage promoted an increase in roughness, thickness, pore area, and a decrease in the pore population on the coatings. The coatings were mainly composed of anatase and rutile TiO₂ phases. Furthermore, the bioactive elements Ca and P were successfully incorporated into the chemical composition of the coating. All coatings presented a hydrophilic behavior.

The coated samples presented higher COF values compared to the metallic substrate. The total rupture of any of the studied coatings was not verified. Adhesive and abrasive wear mechanisms, with the formation of a third body, were identified as responsible for the wear of the samples. The thinner coatings presented lower wear rates, combined with the wear rate results, the partial delamination of the TiAM-PEO_{300v} ($23.83 \pm 1.5 \mu\text{m}$) sample, which resulted in a partial breakage of the coating, demonstrates that the coatings of the TiAM-PEO_{200v} ($2.05 \pm 0.13 \mu\text{m}$) and TiAM-PEO_{250v} ($4.50 \pm 0.33 \mu\text{m}$) samples had better wear resistance. The main wear mechanism found on the substrate was abrasive wear. In PEO coatings, microcracks, generated by crack propagation, which are typical of brittle materials, were the main wear mechanisms detected.

The samples TiAM-PEO_{200v} and TiAM-PEO_{250v} presented denser and thinner coatings, with a hollow structure, compared to the coating formed on the TiAM-PEO_{300v} sample, which presented thicker coatings, with a spongy structure mixed with the hollow structure.

The refined martensitic microstructure obtained from the L-PFL technique provides thicker coatings than those obtained on the Ti-6Al-4V commercial alloy and improves the wear resistance of all PEO coatings studied; this is such a positive and promising behavior for application in the area of metallic implants and consequently in the tissue engineering.

Author Contributions: P.B.S., V.V.d.C., E.K.B. and G.A.L.: conceptualization, investigation, writing—review and editing. C.A. and A.M.H.d.A.: investigation, writing—review and editing. A.L.J. and É.S.N.L.: conceptualization, resources, supervision. C.d.F.M.: supervision, writing, conceptualization, resources, supervision, review and editing. All authors have read and agreed to the published version of the manuscript.

Funding: All work presented can only be produced through the support of the Brazilian government through the National Council for Scientific and Technological Development (CNPq) (408366/2018-4). The authors acknowledge CAPES-PROEX—23038.000341/2019-71, Research Support Foundation of the State of RS (FAPERGS) (19/2551-0000699-3 and 19/2551-0002280-8) and São Paulo Research Foundation (FAPESP) (2019/15441-9 and 2020/05612-8). P.B. Santos acknowledges CAPES (88887.372291/2019-00), V.V. Castro acknowledges CNPq (166262/2018-8) and C.F. Malfatti acknowledges CNPq (Grant 307723/2018-6).

Institutional Review Board Statement: Not applicable.

Informed Consent Statement: Not applicable.

Data Availability Statement: Not applicable.

Conflicts of Interest: The authors declare no conflict of interest.

References

1. Ngo, T.D.; Kashani, A.; Imbalzano, G.; Nguyen, K.T.Q.; Hui, D. Additive Manufacturing (3D Printing): A Review of Materials, Methods, Applications and Challenges. *Compos. Part B Eng.* **2018**, *143*, 172–196. [\[CrossRef\]](#)
2. *NBRISO/ASTM52900*; Additive Manufacturing—General Principles—Terminology. ISO: Rio de Janeiro, Brazil, 2015.
3. Atzeni, E.; Salmi, A. Study on Unsupported Overhangs of AlSi10Mg Parts Processed by Direct Metal Laser Sintering (DMLS). *J. Manuf. Processes* **2015**, *20*, 500–506. [\[CrossRef\]](#)
4. Murr, L.E.; Gaytan, S.M.; Ramirez, D.A.; Martinez, E.; Hernandez, J.; Amato, K.N.; Shindo, P.W.; Medina, F.R.; Wicker, R.B. Metal Fabrication by Additive Manufacturing Using Laser and Electron Beam Melting Technologies. *J. Mater. Sci. Technol.* **2012**, *28*, 1–14. [\[CrossRef\]](#)
5. Yao, J.; Ding, R.; Li, K.; Du, B.; Zhao, L.; Yuan, Y. Study on the impact behavior of arch micro-strut (ARCH) lattice structure by selective laser melting (SLM). *Rapid Prototyp. J.* **2022**; *in press*. [\[CrossRef\]](#)
6. Linares, J.-M.; Chaves-Jacob, J.; Lopez, Q.; Sprauel, J.-M. Fatigue life optimization for 17-4Ph steel produced by selective laser melting. *Rapid Prototyp. J.* **2022**, *28*, 1182–1192. [\[CrossRef\]](#)
7. Giganto, S.; Martínez-Pellitero, S.; Cuesta, E.; Zapico, P.; Barreiro, J. Proposal of design rules for improving the accuracy of selective laser melting (SLM) manufacturing using benchmarks parts. *Rapid Prototyp. J.* **2022**, *28*, 1129–1143. [\[CrossRef\]](#)
8. Khorasani, M.; Ghasemi, A.; Rolfe, B.; Gibson, I. Additive manufacturing a powerful tool for the aerospace industry. *Rapid Prototyp. J.* **2022**, *28*, 87–100. [\[CrossRef\]](#)
9. Wei, D.; Zhou, Y.; Jia, D.; Wang, Y. Characteristic and in Vitro Bioactivity of a Microarc-Oxidized TiO₂-Based Coating after Chemical Treatment. *Acta Biomater.* **2007**, *3*, 817–827. [\[CrossRef\]](#)
10. Becerikli, M.; Kopp, A.; Kröger, N.; Bodrova, M.; Wallner, C.; Wagner, J.M.; Dadras, M.; Jettkant, B.; Pöhl, F.; Lehnhardt, M.; et al. A Novel Titanium Implant Surface Modification by Plasma Electrolytic Oxidation (PEO) Preventing Tendon Adhesion. *Mater. Sci. Eng. C* **2021**, *123*, 112030. [\[CrossRef\]](#)
11. Ciocca, L.; Fantini, M.; De Crescenzo, F.; Corinaldesi, G.; Scotti, R. Direct Metal Laser Sintering (DMLS) of a Customized Titanium Mesh for Prosthetically Guided Bone Regeneration of Atrophic Maxillary Arches. *Med. Biol. Eng. Comput.* **2011**, *49*, 1347–1352. [\[CrossRef\]](#)
12. Ganesh, B.K.C.; Ramanaiah, N.; Rao, P.V.C. Effect of Surface Treatment on Tribological Behavior of Ti-6Al-4V Implant Alloy. *J. Miner. Mater. Charact. Eng.* **2012**, *11*, 735. [\[CrossRef\]](#)
13. Long, M.; Rack, H.J. Friction and Surface Behavior of Selected Titanium Alloys during Reciprocating-Sliding Motion. *Wear* **2001**, *249*, 157–167. [\[CrossRef\]](#)

14. Bartolomeu, F.; Buciumeanu, M.; Pinto, E.; Alves, N.; Silva, F.S.; Carvalho, O.; Miranda, G. Wear Behavior of Ti6Al4V Biomedical Alloys Processed by Selective Laser Melting, Hot Pressing and Conventional Casting. *Trans. Nonferrous Met. Soc. China* **2017**, *27*, 829–838. [[CrossRef](#)]
15. Singh, S.; Pandey, K.K.; Islam, A.; Keshri, A.K. Corrosion Behaviour of Plasma Sprayed Graphene Nanoplatelets Reinforced Hydroxyapatite Composite Coatings in Simulated Body Fluid. *Ceram. Int.* **2020**, *46*, 13539–13548. [[CrossRef](#)]
16. Singh, G.; Sharma, N.; Kumar, D.; Hegab, H. Design, Development and Tribological Characterization of Ti–6Al–4V/Hydroxyapatite Composite for Bio-Implant Applications. *Mater. Chem. Phys.* **2020**, *243*, 122662. [[CrossRef](#)]
17. Costa, A.I.; Sousa, L.; Alves, A.C.; Toptan, F. Tribocorrosion Behaviour of Bio-Functionalized Porous Ti Surfaces Obtained by Two-Step Anodic Treatment. *Corros. Sci.* **2020**, *166*, 108467. [[CrossRef](#)]
18. Çomaklı, O.; Yazıcı, M.; Kovacı, H.; Yetim, T.; Yetim, A.F.; Çelik, A. Tribological and Electrochemical Properties of TiO₂ Films Produced on Cp-Ti by Sol-Gel and SILAR in Bio-Simulated Environment. *Surf. Coat. Technol.* **2018**, *352*, 513–521. [[CrossRef](#)]
19. Bertuccioli; Garzoni; Martini; Morri; Rondelli Plasma Electrolytic Oxidation (PEO) Layers from Silicate/Phosphate Baths on Ti-6Al-4V for Biomedical Components: Influence of Deposition Conditions and Surface Finishing on Dry Sliding Behaviour. *Coatings* **2019**, *9*, 614. [[CrossRef](#)]
20. Simchen, F.; Sieber, M.; Lampke, T. Electrolyte Influence on Ignition of Plasma Electrolytic Oxidation Processes on Light Metals. *Surf. Coat. Technol.* **2017**, *315*, 205–213. [[CrossRef](#)]
21. Durdu, S.; Deniz, Ö.F.; Kutbay, I.; Usta, M. Characterization and Formation of Hydroxyapatite on Ti6Al4V Coated by Plasma Electrolytic Oxidation. *J. Alloy. Compd.* **2013**, *551*, 422–429. [[CrossRef](#)]
22. Parfenov, E.V.; Parfenova, L.V.; Dyakonov, G.S.; Danilko, K.V.; Mukaeva, V.R.; Farrakhov, R.G.; Lukina, E.S.; Valiev, R.Z. Surface Functionalization via PEO Coating and RGD Peptide for Nanostructured Titanium Implants and Their in Vitro Assessment. *Surf. Coat. Technol.* **2019**, *357*, 669–683. [[CrossRef](#)]
23. Santos-Coquillat, A.; Martínez-Campos, E.; Mohedano, M.; Martínez-Corriá, R.; Ramos, V.; Arrabal, R.; Matykina, E. In Vitro and in Vivo Evaluation of PEO-Modified Titanium for Bone Implant Applications. *Surf. Coat. Technol.* **2018**, *347*, 358–368. [[CrossRef](#)]
24. Aliasghari, S.; Skeldon, P.; Thompson, G.E. Plasma Electrolytic Oxidation of Titanium in a Phosphate/Silicate Electrolyte and Tribological Performance of the Coatings. *Appl. Surf. Sci.* **2014**, *316*, 463–476. [[CrossRef](#)]
25. Alves, S.A.; Bayón, R.; de Viteri, V.S.; Garcia, M.P.; Igartua, A.; Fernandes, M.H.; Rocha, L.A. Tribocorrosion Behavior of Calcium- and Phosphorous-Enriched Titanium Oxide Films and Study of Osteoblast Interactions for Dental Implants. *J. Bio Tribo Corros.* **2015**, *1*, 23. [[CrossRef](#)]
26. Chen, C.; Dong, Q.; Yu, H.; Wang, X.; Wang, D. Microstructure of Porous TiO₂ Coating on Pure Ti by Micro-Arc Oxidation. *Adv. Eng. Mater.* **2006**, *8*, 754–759. [[CrossRef](#)]
27. Santos, P.B.; Baldin, E.K.; Krieger, D.A.; de Castro, V.V.; Aguzzoli, C.; Fonseca, J.C.; Rodrigues, M.; Lopes, M.A.; de Fraga Malfatti, C. Wear Performance and Osteogenic Differentiation Behavior of Plasma Electrolytic Oxidation Coatings on Ti-6Al-4V Alloys: Potential Application for Bone Tissue Repairs. *Surf. Coat. Technol.* **2021**, *417*, 127179. [[CrossRef](#)]
28. Yu, J.-M.; Choe, H.-C. Morphology Changes and Bone Formation on PEO-Treated Ti-6Al-4V Alloy in Electrolyte Containing Ca, P, Sr, and Si Ions. *Appl. Surf. Sci.* **2019**, *477*, 121–130. [[CrossRef](#)]
29. Fazel, M.; Salimijazi, H.R.; Shamanian, M.; Minneboo, M.; Modaresifar, K.; van Hengel, I.A.J.; Fratila-Apachitei, L.E.; Apachitei, I.; Zadpoor, A.A. Osteogenic and Antibacterial Surfaces on Additively Manufactured Porous Ti-6Al-4V Implants: Combining Silver Nanoparticles with Hydrothermally Synthesized HA Nanocrystals. *Mater. Sci. Eng. C* **2021**, *120*, 111745. [[CrossRef](#)]
30. Yan, X.; Chen, C.; Bolot, R.; Ma, W.; Deng, C.; Wang, J.; Ren, Z.; Liao, H.; Liu, M. Improvement of Tribological Performance by Micro-Arc Oxidation Treatment on Selective Laser Melting Ti6Al4V Alloy. *Mater. Res. Express* **2019**, *6*, 096509. [[CrossRef](#)]
31. Exley, C. The Toxicity of Aluminium in Humans. *Morphologie* **2016**, *100*, 51–55. [[CrossRef](#)]
32. Yellamma, K.; Saraswathamma, S.; Kumari, B.N. Cholinergic System under Aluminium Toxicity in Rat Brain. *Toxicol. Int.* **2010**, *17*, 106–112. [[CrossRef](#)] [[PubMed](#)]
33. Hussein, R.O.; Nie, X.; Northwood, D.O. An Investigation of Ceramic Coating Growth Mechanisms in Plasma Electrolytic Oxidation (PEO) Processing. *Electrochim. Acta* **2013**, *112*, 111–119. [[CrossRef](#)]
34. Hussein, R.O.; Nie, X.; Northwood, D.O.; Yerokhin, A.; Matthews, A. Spectroscopic Study of Electrolytic Plasma and Discharging Behaviour during the Plasma Electrolytic Oxidation (PEO) Process. *J. Phys. D Appl. Phys.* **2010**, *43*, 105203. [[CrossRef](#)]
35. Han, I.; Choi, J.H.; Zhao, B.H.; Baik, H.K.; Lee, I.-S. Changes in Anodized Titanium Surface Morphology by Virtue of Different Unipolar DC Pulse Waveform. *Surf. Coat. Technol.* **2007**, *201*, 5533–5536. [[CrossRef](#)]
36. Wu, G.; Wang, Y.; Sun, M.; Zhang, Q.; Yao, J. Influence of Microstructure of TC4 Substrate on the MAO Coating. *Surf. Eng.* **2020**, *36*, 827–836. [[CrossRef](#)]
37. Longhitano, G.A.; Arenas, M.A.; Conde, A.; Larosa, M.A.; Jardini, A.L.; de Carvalho Zavaglia, C.A.; Damboreneac, J.J. Heat Treatments Effects on Functionalization and Corrosion Behavior of Ti-6Al-4V ELI Alloy Made by Additive Manufacturing. *J. Alloy. Compd.* **2018**, *765*, 961–968. [[CrossRef](#)]
38. Baldin, E.K.; Santos, P.B.; de Castro, V.V.; Aguzzoli, C.; Maurmann, N.; Girón, J.; Pranke, P.; de Fraga Malfatti, C. Plasma Electrolytic Oxidation (PEO) Coated CP-Ti: Wear Performance on Reciprocating Mode and Chondrogenic–Osteogenic Differentiation. *J. Bio Tribo Corros.* **2021**, *8*, 29. [[CrossRef](#)]
39. Jiang, Y.; Wang, J.; Hu, B.; Yao, Z.; Xia, Q.; Jiang, Z. Preparation of a Novel Yellow Ceramic Coating on Ti Alloys by Plasma Electrolytic Oxidation. *Surf. Coat. Technol.* **2016**, *307*, 1297–1302. [[CrossRef](#)]

40. Durdu, S.; Usta, M.; Berkem, A.S. Bioactive Coatings on Ti6Al4V Alloy Formed by Plasma Electrolytic Oxidation. *Surf. Coat. Technol.* **2016**, *301*, 85–93. [[CrossRef](#)]
41. Yao, Z.Q.; Ivanisenko, Y.; Diemant, T.; Caron, A.; Chuvilin, A.; Jiang, J.Z.; Valiev, R.Z.; Qi, M.; Fecht, H.-J. Synthesis and Properties of Hydroxyapatite-Containing Porous Titania Coating on Ultrafine-Grained Titanium by Micro-Arc Oxidation. *Acta Biomater.* **2010**, *6*, 2816–2825. [[CrossRef](#)]
42. Aliofkhaezai, M.; Macdonald, D.D.; Matykina, E.; Parfenov, E.V.; Egorkin, V.S.; Curran, J.A.; Troughton, S.C.; Sinebryukhov, S.L.; Gnedenkov, S.V.; Lampke, T.; et al. Review of Plasma Electrolytic Oxidation of Titanium Substrates: Mechanism, Properties, Applications and Limitations. *Appl. Surf. Sci. Adv.* **2021**, *5*, 100121. [[CrossRef](#)]
43. Durdu, S.; Usta, M. The Tribological Properties of Bioceramic Coatings Produced on Ti6Al4V Alloy by Plasma Electrolytic Oxidation. *Ceram. Int.* **2014**, *40*, 3627–3635. [[CrossRef](#)]
44. Martin, J.; Nominé, A.; Ntomprougkidis, V.; Migot, S.; Bruyère, S.; Soldera, F.; Belmonte, T.; Henrion, G. Formation of a Metastable Nanostructured Mullite during Plasma Electrolytic Oxidation of Aluminium in “Soft” Regime Condition. *Mater. Des.* **2019**, *180*, 107977. [[CrossRef](#)]
45. Hwang, I.-J.; Choe, H.-C. Hydroxyapatite Coatings Containing Zn and Si on Ti-6Al-4V Alloy by Plasma Electrolytic Oxidation. *Appl. Surf. Sci.* **2018**, *432*, 337–346. [[CrossRef](#)]
46. Matykina, E.; Arrabal, R.; Skeldon, P.; Thompson, G.E. Transmission Electron Microscopy of Coatings Formed by Plasma Electrolytic Oxidation of Titanium. *Acta Biomater.* **2009**, *5*, 1356–1366. [[CrossRef](#)]
47. Yu, S.; Yu, Z.; Wang, G.; Han, J.; Ma, X.; Dargusch, M.S. Biocompatibility and Osteoconduction of Active Porous Calcium–Phosphate Films on a Novel Ti–3Zr–2Sn–3Mo–25Nb Biomedical Alloy. *Colloids Surf. B Biointerfaces* **2011**, *85*, 103–115. [[CrossRef](#)]
48. dos Santos, A.; Araujo, J.R.; Landi, S.M.; Kuznetsov, A.; Granjeiro, J.M.; de Sena, L.Á.; Achete, C.A. A Study of the Physical, Chemical and Biological Properties of TiO₂ Coatings Produced by Micro-Arc Oxidation in a Ca–P-Based Electrolyte. *J. Mater. Sci. Mater. Med.* **2014**, *25*, 1769–1780. [[CrossRef](#)]
49. Ríos, J.M.; Quintero, D.; Castaño, J.G.; Echeverría, F.; Gómez, M.A. Comparison among the Lubricated and Unlubricated Tribological Behavior of Coatings Obtained by PEO on the Ti6Al4V Alloy in Alkaline Solutions. *Tribol. Int.* **2018**, *128*, 1–8. [[CrossRef](#)]
50. de Viteri, V.S.; Bayón, R.; Igartua, A.; Barandika, G.; Moreno, J.E.; Peremarch, C.P.-J.; Pérez, M.M. Structure, Tribocorrosion and Biocide Characterization of Ca, P and I Containing TiO₂ Coatings Developed by Plasma Electrolytic Oxidation. *Appl. Surf. Sci.* **2016**, *367*, 1–10. [[CrossRef](#)]
51. Qian, J.; Yin, X.; Wang, N.; Liu, L.; Xing, J. Preparation and Tribological Properties of Stearic Acid-Modified Hierarchical Anatase TiO₂ Microcrystals. *Appl. Surf. Sci.* **2012**, *258*, 2778–2782. [[CrossRef](#)]
52. Chen, H.-T.; Chung, C.-J.; Yang, T.-C.; Tang, C.-H.; He, J.-L. Microscopic Observations of Osteoblast Growth on Micro-Arc Oxidized β Titanium. *Appl. Surf. Sci.* **2013**, *266*, 73–80. [[CrossRef](#)]
53. Chung, C.-J.; Su, R.-T.; Chu, H.-J.; Chen, H.-T.; Tsou, H.-K.; He, J.-L. Plasma Electrolytic Oxidation of Titanium and Improvement in Osseointegration. *J. Biomed. Mater. Res. Part B Appl. Biomater.* **2013**, *101B*, 1023–1030. [[CrossRef](#)] [[PubMed](#)]
54. Mashtalyar, D.V.; Nadaraia, K.V.; Imshinetskiy, I.M.; Belov, E.A.; Filonina, V.S.; Suchkov, S.N.; Gnedenkov, S.V. Composite coatings formed on Ti by PEO and fluoropolymer treatment. *Appl. Surf. Sci.* **2021**, *536*, 147976. [[CrossRef](#)]
55. Han, J.; Cheng, Y.; Tu, W.; Zhan, T.-Y.; Cheng, Y. The Black and White Coatings on Ti-6Al-4V Alloy or Pure Titanium by Plasma Electrolytic Oxidation in Concentrated Silicate Electrolyte. *Appl. Surf. Sci.* **2018**, *428*, 684–697. [[CrossRef](#)]
56. Kumari, R.; Blawert, C.; Majumdar, J.D. Microstructures and Properties of Plasma Electrolytic Oxidized Ti Alloy (Ti-6Al-4V) for Bio-Implant Application. *Met. Mat. Trans. A* **2016**, *47*, 788–800. [[CrossRef](#)]
57. Santos-Coquillat, A.; Mohedano, M.; Martinez-Campos, E.; Arrabal, R.; Pardo, A.; Matykina, E. Bioactive Multi-Elemental PEO-Coatings on Titanium for Dental Implant Applications. *Mater. Sci. Eng. C* **2019**, *97*, 738–752. [[CrossRef](#)]
58. Wang, S.; Liu, Y.; Zhang, C.; Liao, Z.; Liu, W. The Improvement of Wettability, Biotribological Behavior and Corrosion Resistance of Titanium Alloy Pretreated by Thermal Oxidation. *Tribol. Int.* **2014**, *79*, 174–182. [[CrossRef](#)]
59. He, J.; Zhou, W.; Zhou, X.; Zhong, X.; Zhang, X.; Wan, P.; Zhu, B.; Chen, W. The Anatase Phase of Nanotopography Titania Plays an Important Role on Osteoblast Cell Morphology and Proliferation. *J. Mater. Sci. Mater. Med.* **2008**, *19*, 3465–3472. [[CrossRef](#)]
60. Gittens, R.A.; Scheideler, L.; Rupp, F.; Hyzy, S.L.; Geis-Gerstorfer, J.; Schwartz, Z.; Boyan, B.D. A Review on the Wettability of Dental Implant Surfaces II: Biological and Clinical Aspects. *Acta Biomater.* **2014**, *10*, 2907–2918. [[CrossRef](#)]
61. Bartolomeu, F.; Sampaio, M.; Carvalho, O.; Pinto, E.; Alves, N.; Gomes, J.R.; Silva, F.S.; Miranda, G. Tribological Behavior of Ti6Al4V Cellular Structures Produced by Selective Laser Melting. *J. Mech. Behav. Biomed. Mater.* **2017**, *69*, 128–134. [[CrossRef](#)]
62. Chen, Y.; Cheng, T.; Nie, X. Wear Failure Behaviour of Titanium-Based Oxide Coatings on a Titanium Alloy under Impact and Sliding Forces. *J. Alloy Compd.* **2013**, *578*, 336–344. [[CrossRef](#)]
63. Longhitano, G.A.; Larosa, M.A.; Jardini, A.L.; Zavaglia, C.A.d.C.; Ierardi, M.C.F. Correlation between Microstructures and Mechanical Properties under Tensile and Compression Tests of Heat-Treated Ti-6Al-4V ELI Alloy Produced by Additive Manufacturing for Biomedical Applications. *J. Mater. Process. Technol.* **2018**, *252*, 202–210. [[CrossRef](#)]
64. Yang, X.; Wang, W.; Ma, W.; Wang, Y.; Yang, J.; Liu, S.; Tang, H. Corrosion and Wear Properties of Micro-Arc Oxidation Treated Ti6Al4V Alloy Prepared by Selective Electron Beam Melting. *Trans. Nonferrous Met. Soc. China* **2020**, *30*, 2132–2142. [[CrossRef](#)]
65. Lawn, B.R.; Borrero-Lopez, O.; Huang, H.; Zhang, Y. Micromechanics of Machining and Wear in Hard and Brittle Materials. *J. Am. Ceram. Soc.* **2021**, *104*, 5–22. [[CrossRef](#)] [[PubMed](#)]

66. Sankara Narayanan, T.S.N.; Kim, J.; Park, H.W. High Performance Corrosion and Wear Resistant Ti-6Al-4V Alloy by the Hybrid Treatment Method. *Appl. Surf. Sci.* **2020**, *504*, 144388. [[CrossRef](#)]
67. Aliofkhaezai, M.; Sabour Rouhaghdam, A.; Shahrabi, T. Abrasive Wear Behaviour of Si₃N₄/TiO₂ Nanocomposite Coatings Fabricated by Plasma Electrolytic Oxidation. *Surf. Coat. Technol.* **2010**, *205*, S41–S46. [[CrossRef](#)]
68. Martin, J.; Nominé, A.; Brochard, F.; Briançon, J.-L.; Noël, C.; Belmonte, T.; Czerwicz, T.; Henrion, G. Delay in Micro-Discharges Appearance during PEO of Al: Evidence of a Mechanism of Charge Accumulation at the Electrolyte/Oxide Interface. *Appl. Surf. Sci.* **2017**, *410*, 29–41. [[CrossRef](#)]